

**Manuscript version: Author's Accepted Manuscript**

The version presented in WRAP is the author's accepted manuscript and may differ from the published version or Version of Record.

**Persistent WRAP URL:**

<http://wrap.warwick.ac.uk/170558>

**How to cite:**

Please refer to published version for the most recent bibliographic citation information. If a published version is known of, the repository item page linked to above, will contain details on accessing it.

**Copyright and reuse:**

The Warwick Research Archive Portal (WRAP) makes this work by researchers of the University of Warwick available open access under the following conditions.

Copyright © and all moral rights to the version of the paper presented here belong to the individual author(s) and/or other copyright owners. To the extent reasonable and practicable the material made available in WRAP has been checked for eligibility before being made available.

Copies of full items can be used for personal research or study, educational, or not-for-profit purposes without prior permission or charge. Provided that the authors, title and full bibliographic details are credited, a hyperlink and/or URL is given for the original metadata page and the content is not changed in any way.

**Publisher's statement:**

Please refer to the repository item page, publisher's statement section, for further information.

For more information, please contact the WRAP Team at: [wrap@warwick.ac.uk](mailto:wrap@warwick.ac.uk).

# Fabrication of Cross-scale Structures by Moiré Effect in Laser Interference Lithography

Mengnan Liu,<sup>1,2,3</sup> Zuobin Wang,<sup>1,2,3,\*</sup> Litong Dong,<sup>1,2,3,\*</sup> Baishun Sun,<sup>1,2</sup> Ying Wang,<sup>1,2,3</sup> Lu Wang,<sup>1,2,3</sup> Zhankun Weng,<sup>1,2,3</sup> Yanling Tian<sup>4</sup>

<sup>1</sup>Changchun University of Science and Technology, International Research Centre for Nano Handling and Manufacturing of China, 7089 Weixing Road, Changchun, China, 130022

<sup>2</sup>Changchun University of Science and Technology, Ministry of Education Key Laboratory for Cross-Scale Micro and Nano Manufacturing, 7089 Weixing Road, Changchun, China, 130022

<sup>3</sup>Zhongshan Institute of Changchun University of Science and Technology, Zhongshan 528437, China

<sup>4</sup>University of Warwick, School of Engineering, Coventry, UK, CV4 7AL

## Corresponding author

\*E-mail address: [wangz@cust.edu.cn](mailto:wangz@cust.edu.cn) (Z. Wang), [donglt@cust.edu.cn](mailto:donglt@cust.edu.cn) (L. Dong)

**Abstract.** This paper presents a method for the fabrication of cross-scale structures using the controllable Moiré effect to break through the scale barriers caused by the spatial distribution in a laser interference lithography (LIL) system. The formation principle of macroscopic Moiré gratings in the LIL system was analyzed as partial wavefront interference introduced by optical components. In this work, an additional lens was used in the improved two-beam LIL system to precisely control the size of Moiré gratings, combined with the intrinsic period in the LIL system to form a cross-scale distribution of light intensity. This method provides a way for the fabrication of cross-scale surface structures by single exposure. Through the double exposure technology, the fabrication of isotropic and anisotropic structures can be achieved flexibly for different applications, such as photonic crystals, self-cleaning surfaces, structural color elements and anti-counterfeiting labels.

## 1 Introduction

In nature, composite surface structures play an important role for enhancing or changing surface functions, such as self-cleaning, antireflection, and structured color [1--4]. The special functions of lotus leaves, rice leaves, moth eyes and other biological organs are due to the special cross-scale structures on their surfaces [5--7]. Optical elements with complex surface structures also have a wide range of applications in plasma, photocatalysis, biosensing, and other areas [8--11]. Complex topographies in in-vivo at micro- and nanoscale can induce cell growth, differentiation, and migration [12--14]. Cross-scale micro- and nanostructures are of great significance in the fields of micro-nano manufacturing, bionics, and biology. Thus, how to fabricate cross-scale structures is an important topic in these fields.

The commonly used fabrication methods of micro- and nanostructures include femtosecond laser machining [15], self-assembly [16], chemical etching [17], electron beam lithography (EBL) [18], and laser interference lithography (LIL) [19, 20]. Among the methods, LIL has the advantages of maskless, high flexibility, large area and low cost. When a multi-beam LIL system is used to fabricate cross-scale structures, the optical system is complicated and difficult to set up [21--23]. A multi-beam LIL system is usually used to fabricate micro and nano structures. Due to the space limitation of building a multi-beam LIL system with the number of required optical components and coherence condition of the light source, there are certain difficulties in the realization of cross-scale structures with both the macroscopic and microcosmic scales. In other words, the multi-beam LIL system configurations can be hardly constructed to achieve the intensity distribution fields at macro-micro scales. The system is also complicated to be set up with precision. Another approach is the generation of cross-scale Moiré fringes using the wavefront curvature and the superimposition of multiple exposures [24]. The macroscopic structures prepared by the multiple exposures of wavefront curvature lead to the uneven distribution of the macroscopic period, and the excessive exposure times affect the integrity and uniformity of the microstructure distribution. While the LIL system is often used to fabricate structures, it is found in our work that the periodic Moiré fringes on the macroscopic scale appear during the light exposure, which breaks through the scale limitation of the LIL system and forms a periodic light intensity distribution on the sub-millimeter or even millimeter scale. Such Moiré effect with macroscopic fringes has its potential to be used as cross-scale surface structures on the nano-milli and micro-milli scales. Therefore, exploring the generation principle of cross-scale Moiré fringes can be a useful approach to fabricate cross-scale structures from a single exposure.

In this work, the generation principle of Moiré effect with macroscopic fringes in an LIL system was analyzed as the thin-film interference when the laser passed through the non-polarization beam splitter. An improved two-beam LIL system was designed to control the Moiré effect to fabricate cross-scale structures with dual periods of macroscopic and microscopic from a single exposure. The designed optical system in the experiment is simple and easy to build. This method avoids the problems of material surface damage and structural shift caused by multiple exposures and developments. The periods of macroscopic and microscopic show good uniformity and consistency. The characteristic parameters and principle of fabricating macroscopic Moiré fringes were discussed. The double-exposure technology was used to generate isotropic and anisotropic cross-scale structures in different distributions via the improved two-beam LIL system. This approach can be used in different applications in bionic manufacturing, optical device manufacturing, holographic imaging.

## **2 Material and methods**

Macroscopic Moiré effect occurs in laser interference. By tracking the propagation path of incident light, it is found that there are additional light spots after the light beam passes through a non-polarization beam splitter (BS), which is the main reason for the macroscopic Moiré effect. The laser beam splitting performance of BS is determined by a layer of sputtered dielectric coating on it. The redundant coherent beams appear when an incident light passes through the BS. There are six main coherent beams come from the air-dielectric partial reflection film interface, dielectric partial reflection film-quartz interface and quartz-anti-reflection coating interface corresponding to the reflected beams and the transmitted beams (Fig. 1). After passing through the focal point of a lens, the incident beam diameter is enlarged as the distance is increased. When the beams pass through the focal point of the plano-convex lens and irradiate on the sample stage surface, they are

always partially overlapped, and the wavefront interference occurs, which causes the generation of Moiré fringes. The generation of Moiré fringes makes the intensity distribution change in light and dark with a large period. Therefore, the Moiré fringes have an impact on the distribution of surface structures.

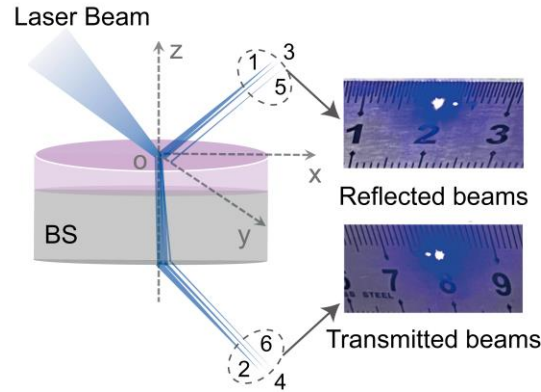


**Fig. 1** Schematic diagram of BS light paths with actual effective transmitted light spots and reflected light spots.

In experiment, the powers of Beam 1 and Beam 2 were both 47.5%, the powers of Beams 3 and 4 were both 2.4%, and the powers of Beam 5 and Beam 6 were both 0.1% of the total laser power, measured by the power meter. The powers of Beam 5 and Beam 6 are well below the exposure threshold and are hardly observable, as can be seen in the insets of Fig.1. Ignoring the effect of Beam 5 and Beam 6 has no impact on the fabrication of micro- and nanostructures. In this case, the Moiré effect in the two-beam LIL system is due to the modulation of the interference field by Beam 3 and Beam 4.

The photoresist was used to record the intensity distribution of two-beam LIL by three main steps for studying the formation of cross-scale structures: 1) spin coating of photoresist on a clean sample (i. e., metal, semiconductor and glass), 2) exposure in the LIL system, and 3) development in resist to obtain the same surface topography as the interference pattern generated by LIL (Figs. 2a-c). The photoresist shows the alternating strong and weak absorbing regions with the light intensity distribution. At the strong absorbing region, the absorbed light intensity reaches the

exposure threshold, causing the chemical structure of the photoresist to change, while the chemical structure of the photoresist in the weak absorbing region does not change. The strong absorbing region of positive photoresist was removed by the resist during the development process, while the negative photoresist showed the opposite phenomenon.

Based on the Moiré effect in the two-beam LIL system, a plano-convex lens was placed in the front of the BS to expand the laser beam (Fig. 2d) and control the cross-scale interference light field (Fig. 2e). The improved two-beam LIL system used Beam 3 and Beam 4 to obtain the macroscopically sized Moiré fringes. The distance from the plano-convex lens to the BS was smaller than its focal length. These coherent beams were symmetrically arranged in the front of the sample stage through two high reflectors (HRs). A rotating table was used as the sample stage to form the anisotropic distributions of structures.

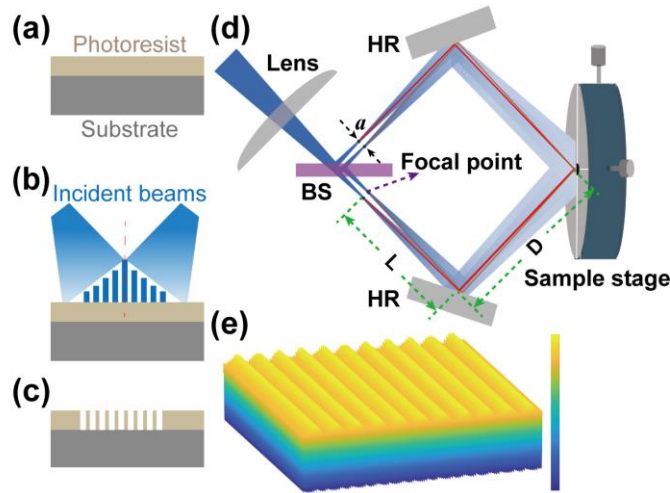


**Fig. 2** The schematic diagram of two-beam LIL. **a** Photoresist coating, **b** exposure, and **c** development. **d** Schematic diagram of the modified two-beam LIL system, and **e** 3D intensity distribution of the improved two-beam LIL system.

### 3 Principle

In the improved two-beam LIL system, the light intensity distribution was regarded as the result of coplanar four-beam interference, generating a complicated interference pattern with the macroscopic stripes and microcosmic lines (Figs. 3a-b). According to previous study [25], the frequency spectrum shows two main frequency distributions corresponding to two periods (Fig. 3c). Among them, the internal distribution provided a main frequency distribution corresponding to the smaller period.

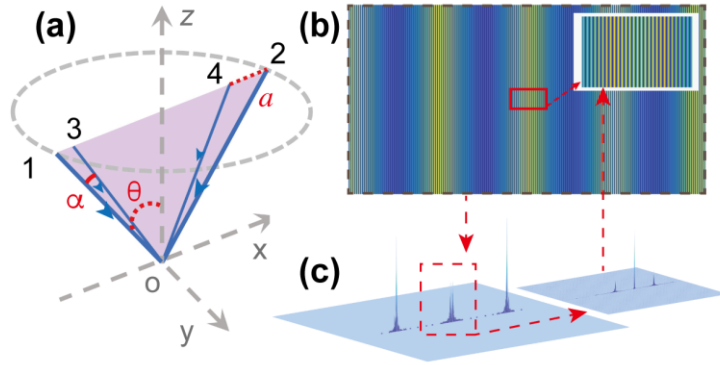


**Fig. 3** The improved two-beam LIL laser interference setting and results. **a** Spatial distribution of incident beams, **b** simulated intensity distribution with macroscopic stripes and microcosmic lines, where the marked area shows the microcosmic lines, and **c** frequency spectra corresponding to the intensity distribution of **b**.

When the polarization directions of all incident beams are not orthogonal, the interference pattern can be regarded as the superimposing of all two-beam pairs. For  $N$ -beam laser interference, it can be described as

$$I(\mathbf{r}) = \sum_{m=1}^N \sum_{n=1}^N |\mathbf{E}_m| |\mathbf{E}_n| \cos\langle \mathbf{E}_m \cdot \mathbf{E}_n \rangle, \quad (1)$$

where  $\mathbf{E}_m$  and  $\mathbf{E}_n$  are the electric field vectors of  $m$ th and  $n$ th beams, respectively.

As shown in Fig. 3a, the four beams are coplanar and symmetrical in the  $x$ - $o$ - $z$  plane after splitting by the BS, namely, their spatial angles are  $0^\circ$ ,  $180^\circ$ ,  $0^\circ$  and  $180^\circ$ , respectively. Beam 1 and Beam 2 have the same incident angle ( $\theta$ ) and the same intensity ( $I_1 = I_2$ ), and the incident

angles of Beam 3 and Beam 4 are both  $\theta - \alpha$ , where  $\alpha$  is the angle between Beam 1 and Beam 3 or Beam 2 and Beam 4, and  $I_3 = I_4$ . The interference intensity distribution in the  $z = 0$  plane is represented by

$$I = I_1^2 + I_2^2 + I_3^2 + I_4^2 + 2I_1I_3\cos[kx(\sin\theta - \sin(\theta - \alpha))] + 2I_2I_4\cos[kx(\sin\theta - \sin(\theta - \alpha))] - 2I_1I_4\cos[kx(\sin\theta + \sin(\theta - \alpha))] - 2I_2I_3\cos[kx(\sin\theta + \sin(\theta - \alpha))] - 2I_1I_2\cos(2kx\sin\theta) - 2I_3I_4\cos[2kx(\sin(\theta - \alpha))], \quad (2)$$

where  $k$  is the wave number ( $k = \lambda/2\pi$ ), and  $\lambda$  is the wavelength of the laser.

The relationship between  $\theta$  and  $a$  is

$$\tan(\theta - \alpha) = \frac{(L+D)\sin\theta - a}{(L+D)\cos\theta}, \quad (3)$$

where  $L$  is the distance between the HR and the focal point,  $D$  is the distance between the HR and the sample stage, and  $a$  is the distance between the focal points of the two beams on the same side in this system (Fig. 2d and Fig. 3a).

According to the spatial distribution of the four beams in Fig. 3a, the intensity  $I$  shows double period distributions in Fig. 4a. To precisely assess the periods of the interference pattern,  $I$  can be divided into six groups of the two-beam interference, which are  $I_{12}$ ,  $I_{13}$ ,  $I_{14}$ ,  $I_{23}$ ,  $I_{24}$ , and  $I_{34}$ . Among them,  $I_{13} = I_{24}$  and  $I_{14} = I_{23}$  due to the symmetrical configuration of the light path system. To simplify the analysis, the same results can be directly superimposed (Figs. 4b-e).



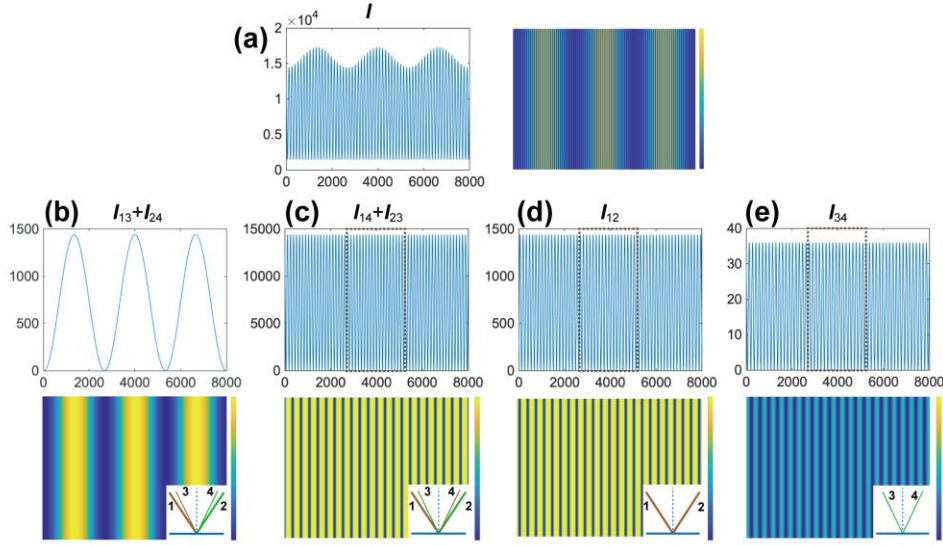


**Fig. 4** Intensity distributions of the improved two-beam LIL. **a** The intensity distribution of  $I$ . **b-e** Separate beam interference distributions of  $I_{13} + I_{24}$ ,  $I_{14} + I_{23}$ ,  $I_{12}$  and  $I_{34}$  corresponding to the incident beams in the bottom right corners.

In Figs. 4b-e, the periods of  $I_{13} + I_{24}$ ,  $I_{14} + I_{23}$ ,  $I_{12}$  and  $I_{34}$  can be expressed as

$$\begin{cases} d_{13+24} = \lambda / (\sin\theta - \sin(\theta - \alpha)) \\ d_{14+23} = \lambda / (\sin\theta + \sin(\theta - \alpha)) \\ d_{12} = \lambda / 2\sin\theta \\ d_{34} = \lambda / 2\sin(\theta - \alpha) \end{cases}. \quad (4)$$

The superimposition of four periods forms the cross-scale period distribution of  $I$ , where  $d_{13+24}$  attributes to the macroscopic stripes, and  $d_{12}$ ,  $d_{14+23}$  and  $d_{34}$  attribute to the microcosmic lines (Fig. 4a). The light intensity of  $I_{12}$  is much higher than those of  $I_{14}$ ,  $I_{23}$  and  $I_{34}$ . As  $\alpha$  approaches to  $0^\circ$ ,  $d_{14+23}$  and  $d_{34}$  are close to the same value of  $d_{12}$ , and the period of  $I$  can be regard as the combination of  $d_{12}$  and  $d_{13+24}$ . When  $\theta$  is fixed, the appropriate values of  $D$ ,  $L$  and  $a$  can make the macroscopic stripes and the microcosmic lines present cross-scale structures. As  $a$  is small enough, the intensity distribution of  $I$  is close to the double-period distribution across scales.

It can be found that the interference light distribution formed by LIL is equivalent to the superimposition of a macroscopic distribution and a microcosmic distribution of interference fields.

In the fabrication, when the exposure light intensity of the microcosmic distribution meets the threshold of the photoresist, the overexposure will occur at the peak of macroscopic distribution. The overexposure will cause the damage or deformation of structures in the peak area of macroscopic distribution, which fabricates cross-scale structures. The light field distribution of double exposure is the superimposition of the light fields  $I_{1st}(x, y)$  and  $I_{2nd}(u, v)$ , where  $I_{2nd}(u, v)$  is obtained by rotating  $I_{1st}(x, y)$  with a certain angle in the  $z = 0$  plane. For the simplified calculation, an identity matrix is used to achieve the clockwise rotation around the center of  $I$  in an angle ( $\beta$ ) to locate  $I_{2nd}$  in the x-y plane, which can be expressed as

$$\begin{pmatrix} u \\ v \end{pmatrix} = \begin{pmatrix} \cos\beta & -\sin\beta \\ \sin\beta & \cos\beta \end{pmatrix} \begin{pmatrix} x \\ y \end{pmatrix}. \quad (5)$$

The intensity distribution of double exposure ( $I_{2-exposure}$ ) is

$$I_{2-exposure}(x, y) = I_{1st}(x, y) + I_{2nd}(x, y). \quad (6)$$

Rotating the single-exposure sample to  $90^\circ$ ,  $60^\circ$ , and  $45^\circ$  around the center, and then performing the second exposure can obtain the anisotropic cross-scale intensity distributions (Figs. 5a-c). Figures 5d-f show a cross-scale anisotropic intensity distribution is composed of anisotropic periodic arrays with the same distribution both at the valley and peak of the macroscopic patterns. The anisotropic distribution and morphology of periodic arrays are changed consistently with the rotation angles (Figs. 5g-i). In the experiment, the overexposure at the peak (yellow area in Fig. 5) of macroscopic patterns was controlled, which caused only the valley area with periodic arrays left after the development. Anisotropic cross-scale structures were fabricated by this method.

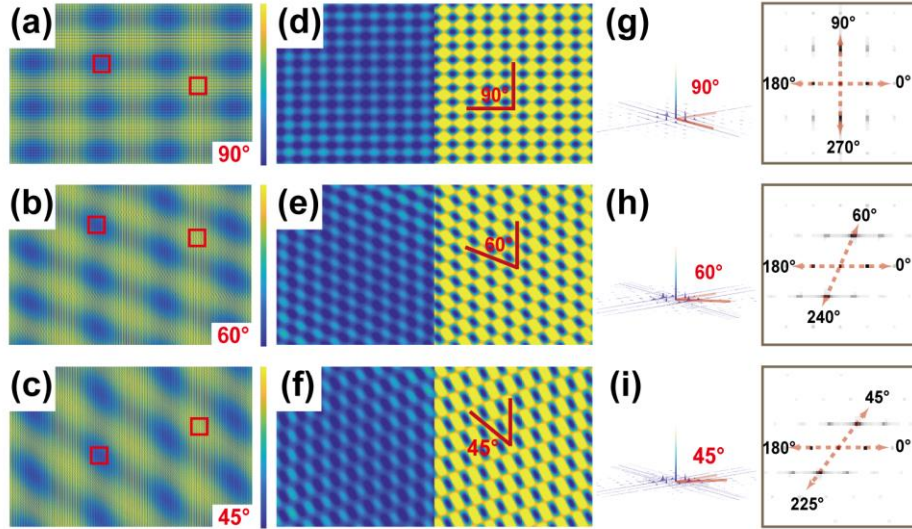


**Fig. 5** Light intensity distributions of double exposures. **a-c** Intensity distributions of double exposures with the rotation angles of 90°, 60°, and 45°. **d-f** The marked areas with periodic arrays at the valleys (blue) and peaks (yellow) of macroscopic patterns. The intensity distributions at the valleys and peaks of macroscopic patterns have the same structures with the periodic arrays, respectively. **g-i** 3D frequency spectra of periodic arrays in **d-f** and frequency distributions in the x-y plane.

#### 4 Results and discussion

To verify the result of theoretical analysis, the designed LIL system corresponding to Fig. 2d was built to fabricate the double-period cross-scale structures. The value of  $(L + D)$  was approximately 1,117.20 mm, and  $a$  was about 1.55 mm. The incident angles of Beams 1 and 2 were designed as 13.21°, while the microscopic period was approximately 1  $\mu\text{m}$ . The period of macroscopic pattern was about 352.69  $\mu\text{m}$ , according to Eq. 3 and Eq. 4. A single-mode diode-pumped solid-state (DPSS) laser with the wavelength of 457 nm (MSL-FN-457-S, CNI) was used as the light source in the LIL system. The positive photoresist (AR-P 3740, Allresist) was used for obtaining the corresponding light fields and forming the periodic micro- and nanostructures after development. A plano-convex lens with the focus of 75 mm was used to expand the laser beams and generate

the modulated large-period structures. The BS front side was coated with a dielectric partial reflection film, and the backside was coated with an anti-reflection coating, and its thickness was 2 mm. The transmittance and reflection ratio was 50:50 at the incident angle of  $45^\circ$ . A scanning electron microscope (SEM; Quanta 250, FEI) and a true color confocal microscope (Axio CSM 700, Carl Zeiss) were employed to evaluate the fabricated structures.

Combining with the designed two-beam LIL system and double exposure method, the cross-scale surface structures were fabricated with the rotation angles of  $90^\circ$ ,  $60^\circ$ , and  $45^\circ$ . When the photoresist was used for exposures, if the valleys of  $I$  reached the material threshold, the strong light intensity at the peak caused the entire peak area's overexposure. This made the peak area of the macroscopic pattern have no distribution of arrays, and there was a periodic anisotropic array at the valley (Figs. 6a-c). The periodic arrays with microcosmic patterns in the marked areas of cross-scale surface structures were different in shapes (Figs. 6d-f). The frequency spectra showed the anisotropic distributions of periodic arrays under the corresponding rotation angles, as shown in Figs. 6g-i.

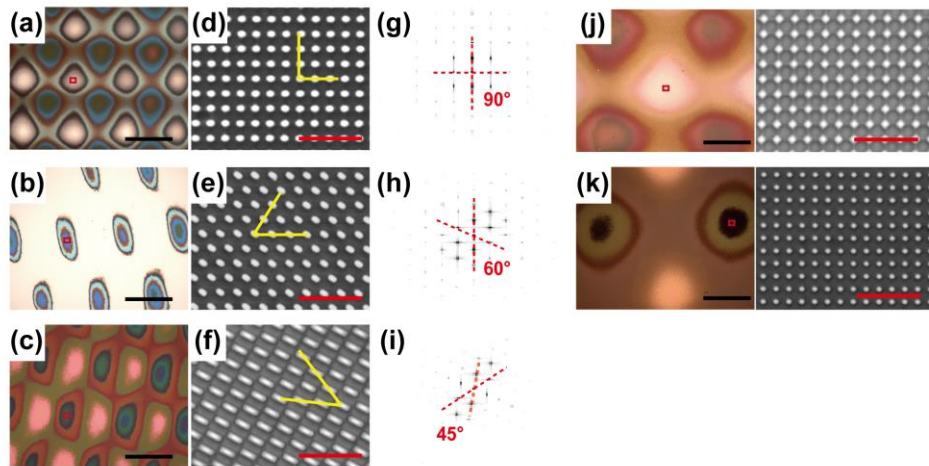


**Fig. 6** Anisotropic cross-scale surface structures fabricated by double exposures with different rotation angles. **a-c**

Surface structures with the rotation angles of  $90^\circ$ ,  $60^\circ$  and  $45^\circ$ . **d-f** The internal structures of indicated areas corresponding to **a-c**, respectively. **g-i** 3D frequency spectra of **d-f**. **j** Cross-scale structure with the macroscopic

period of 1,046.66  $\mu\text{m}$  and the microcosmic period of 1.04  $\mu\text{m}$ . **k** Cross-scale structure with the macroscopic period of 1,271.60  $\mu\text{m}$  and the microcosmic period of 1.21  $\mu\text{m}$ . Black scale bar = 300  $\mu\text{m}$ . Red scale bar = 4  $\mu\text{m}$ .

The macroscopic period in the improved two-beam LIL system was about 343.25  $\mu\text{m}$  measured by true color confocal microscope (Fig. 6a). The microcosmic period was about 931.75 nm measured by SEM (Fig. 6d). The designed microcosmic and macroscopic periods of double-period structures were 1  $\mu\text{m}$  and 352.69  $\mu\text{m}$ , respectively. The improved two-beam LIL system fabricated the cross-scale structures with both micrometer arrays and sub-millimeter arrays. The double exposure method realized the anisotropic distributions of structures according to the rotation angles, which increased the degree of freedom for the fabrication of cross-scale structures.

According to Eq. 3 and Eq. 4, the key factors for controlling the periods of cross-scale structures are  $\lambda$ ,  $\theta$ ,  $a$  and  $(L + D)$ . Among them,  $a$  is related to the parameters of the BS, which can be changed by different types of lenses. The value of  $(L + D)$  can be controlled by changing the distance between the focal point of lens, HR and sample stage in the improved two-beam LIL system. According to Eq. 3,  $\alpha$  is determined by  $(L + D)$  when  $\theta$  is not changed. Furthermore, the  $\theta$  and  $\alpha$  influence the microcosmic period of cross-scale structures together. In the method, the double-period structures with different periods can be fabricated only by changing the value of  $(L + D)$  while keeping the incident angle constant (Figs. 6j-k). The cross-scale structures in Figs. 6j-k are fabricated by the improved two-beam LIL system via the double exposure method with the rotation angle of  $90^\circ$ . The periods of the cross-scale structure in Fig. 6j are 1,046.66  $\mu\text{m}$  and 1.04  $\mu\text{m}$ , and the periods in Fig. 6k are 1,271.60  $\mu\text{m}$  and 1.21  $\mu\text{m}$ . The designed microcosmic periods of Fig. 6j and Fig. 6a are both 1  $\mu\text{m}$ . By changing the value of  $(L + D)$  from 1,117.20 mm to 3369.57 mm, the designed macroscopic periods of Fig. 6j and Fig. 6a are 352.69  $\mu\text{m}$  and 1050  $\mu\text{m}$ , respectively. The cross-scale structure with micro scale and milli scale can be easily achieved by changing the value of  $(L + D)$ . The error mainly came from the deviation of the optical path

generated during the construction of two-beam LIL system. The macroscopic period of structures can be precisely changed without changing the microcosmic period in this work.

## 5 Conclusion

In summary, this work presented a method for the fabrication of cross-scale structures by tuning the Moiré effect in a two-beam LIL system. In this work, it was found that the Moiré effect was a wavefront interference generated by the incident light passing through the BS element through tracking the optical path in the LIL system. On the other hand, the Moiré effect was exploited to break through the scale barriers caused by the spatial distribution in the LIL system. This method provides a way for the fabrication of cross-scale surface structures by single exposure. By adjusting the spatial distances of the lens and other components, the macroscopic period of Moiré fringes and intrinsic period of the two-beam fringes can be controlled quantitatively on the nano-micro, nano-milli and micro-milli scales. Moreover, cross-scale structures with anisotropic distributions and morphologies can be easily determined using the variable rotation angle of the double-exposure technique. This approach can also be used to optimize multi-beam LIL systems, and give the optical systems new design ideas to help achieve more complex structures according to different applications. It enables the fabrication of surface structures from microcosmic patterns to macroscopic patterns, which provides a new way for the design and fabrication of functional surface structures.

**Acknowledgments** This work was supported by National Natural Science Foundation Program of China (grant numbers 62175020, 61964007 and 62175019), EU H2020 Program (grant numbers MNR4SCell No. 734174, NanoStencil No. 767285), Jilin Provincial Science and Technology Program (grant numbers 20210101393JC, 2020C022-1 and 20210101069JC), Jilin Province

Education Department Program (grant number JJKH20210833KJ), and “111” Project of China (grant number D17017). This work was also supported by China Scholarship Council (CSC, grant number 202007585008).

## References

1. M. J. Hancock, K. Sekeroglu, M. C. Demirel: *Adv Funct Mater* **22**, 22 (2012).
2. Z. Zhang, B. Chen, C. Lu, H. Wu, H. Wu, S. Jiang, G. Chai: *Compos. Struct.* **180**, 933 (2017).
3. H. Chen, P. Zhang, L. Zhang, H. Liu, Y. Jiang, D. Zhang, Z. Han, L. Jiang: *Nature* **532**, 85 (2016).
4. Y. Zeng, X. F. Chen, Z. Yi, Y. Yi, X. Xu: *Appl. Surf. Sci.* **441**, 40 (2018).
5. K. Liu, L. Jiang: *Annu. Rev. Mater. Res.* **42**, 231 (2012).
6. D. Wu, J. N. Wang, S. Z. Wu, Q. D. Chen, S. Zhao, H. Zhang, H. B. Sun, L. Jiang: *Adv. Funct. Mater.* **21**, 2927 (2011).
7. J. Xu, Z. Wang, Z. Zhang, D. Wang, Z. Weng: *J. Appl. Phys.* **115**, 203101 (2014).
8. K. Wilson, C. A. Marocico, E. Pedrueza-Villalmanzo, C. Smith, C. Hrelescu, A. Louise Bradley: *Nanomaterials* **9**, 963 (2019).
9. J. Liu, H. Liu, X. Zuo, F. Wen, H. Jiang, H. Cao, Y. Pei: *Mater. Lett.* **254**, 448 (2019).
10. K. Chen, L. Li: *Adv. Mater.* **31**, 1901115 (2019).
11. J. Hasan, S. Jain, R. Padmarajan, S. Purighalla, V. K. Sambandamurthy, K. Chatterjee: *Mater. Des.* **140**, 332 (2018).
12. J. Baek, S. Y. Cho, H. Kang, H. Ahn, W. Bin Jung, Y. Cho, E. Lee, S. W. Cho, H. T. Jung, S. G. Im: *ACS Appl. Mater. Interfaces* **10**, 33891 (2018).
13. J. Kim, K. Yang, K. Jung, E. Ko, J. Kim, K. I. Park, S. W. Cho: *ACS Appl. Mater. Interfaces* **5**, 10529 (2013).
14. S. Shi, Q. Peng, X. Shao, J. Xie, S. Lin, T. Zhang, Q. Li, X. Li, and Y. Lin, *ACS Appl. Mater. Interfaces* **8**, 19353 (2016).
15. G. Schnell, U. Duenow, H. Seitz: *Materials*. **13**, 969 (2020).

16. M. Grzelczak, J. Vermant, E. M. Furst, L. M. Liz-marza: ACS Nano **4**, 3591 (2010).
17. M. Jin, Y. Shen, X. Luo, J. Tao, Y. Xie, H. Chen, Y. Wu: Appl. Surf. Sci. **455**, 883 (2018).
18. T. L. Temple, D. M. Bagnall: J. Appl. Phys. **109**, 084343 (2011).
19. W. Li, Z. Wang, D. Wang, Z. Zhang, L. Zhao, D. Li, R. Qiu, C. Maple: Opt. Eng. **53**, 034109 (2014).
20. F. Pirani, A. Angelini, S. Ricciardi, F. Frascella, E. Descrovi: Appl. Phys. Lett. **110**, 101603 (2017).
21. Z. Zhang, L. Dong, Y. Ding, L. Li, Z. Weng, Z. Wang: Opt. Express **25**, 29135 (2017).
22. L. Dong, Z. Zhang, R. Ding, L. Wang, M. Liu, Z. Weng, Z. Wang, D. Li: Surf. Coatings Technol. **372**, 434 (2019).
23. L. Dong, Z. Zhang, L. Wang, Z. Weng, M. Ouyang, Y. Fu, J. Wang, D. Li, Z. Wang: Appl. Opt. **58**, 6706 (2019).
24. A. A. Ushkov, I. Verrier, T. Kampfe, Y. Jourlin: Opt. Express **28**, 16453 (2020).
25. M. Liu, L. Dong, Z. Zhang, L. Li, L. Wang, Z. Song, Z. Weng, X. Han, L. Zhou, Z. Wang: Appl. Phys. Express **12**, 096503 (2019).